Chapter 4
Photopolymerization Processes

4.1 Introduction

Photopolymerization processes make use of liquid, radiation curable resins, or photopolymers as their primary materials. Most photopolymers react to radiation in the ultraviolet (UV) range of wavelengths, but some visible light systems are used as well. Upon irradiation, these materials undergo a chemical reaction to become solid. This reaction is called photopolymerization, and is typically complex, involving many chemical participants.

Photopolymers were developed in the late 1960s and soon became widely applied in several commercial areas, most notably the coating and printing industry. Many of the glossy coatings on paper and cardboard, for example, are photopolymers. Additionally, photo-curable resins are used in dentistry, such as for sealing the top surfaces of teeth to fill in deep grooves and prevent cavities. In these applications, coatings are cured by radiation that blankets the resin without the need for patterning either the material or the radiation. This changed with the introduction of stereolithography.

In the mid-1980s, Charles (Chuck) Hull was experimenting with UV curable materials by exposing them to a scanning laser, similar to the system found in laser printers. He discovered that solid polymer patterns could be produced. By curing one layer over a previous layer, he could fabricate a solid 3D part. This was the beginning of stereolithography (SL) technology. The company 3D Systems was created shortly thereafter to market SL machines as "rapid prototyping" machines to the product development industry. Since then, a wide variety of SL-related processes and technologies has been developed.

Various types of radiation may be used to cure commercial photopolymers, including gamma rays, X-rays, electron beams, UV, and in some cases visible light. In SL systems, UV and visible light radiation are used most commonly. In the microelectronics industry, photomask materials are often photopolymers and are typically irradiated using far UV and electron beams. In contrast, the field of dentistry uses visible light predominantly.

I. Gibson, D.W. Rosen, and B. Stucker, *Additive Manufacturing Technologies*,
DOI 10.1007/978-1-4419-1120-9_4,

Two primary configurations were developed for photopolymerization processes in a vat, plus one additional configuration that has seen some research interest. Although photopolymers are also used in some ink-jet printing processes, this method of line-wise processing is not covered in this chapter, as the basic processing steps are more similar to the printing processes covered in Chap. 7. The configurations discussed in this chapter include:

- *Vector scan*, or point-wise, approaches typical of commercial SL machines
- *Mask projection*, or layer-wise, approaches, that irradiate entire layers at one time, and
- *Two-photon* approaches that are essentially high resolution point-by-point approaches

These three configurations are shown schematically in Fig. 4.1. Note that in the vector scan and two-photon approaches, scanning laser beams are needed, while the

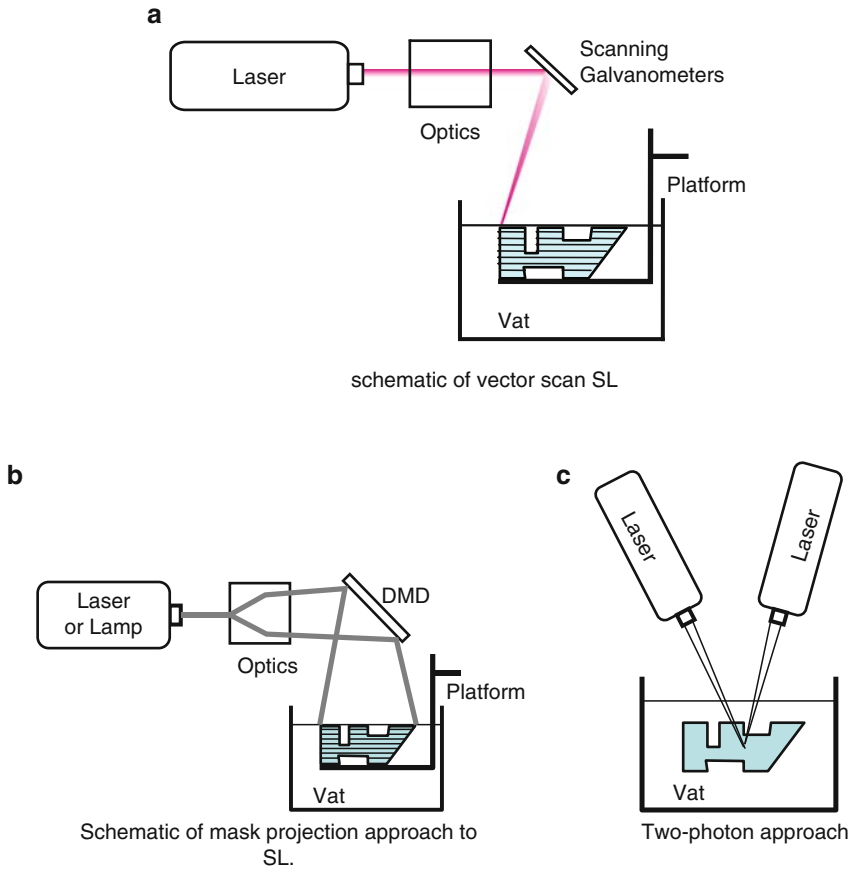

Fig. 4.1 Schematic diagrams of three approaches to photopolymerization processes

mask projection approach utilizes a large radiation beam that is patterned by another device, in this case a Digital Micromirror Device™ (DMD). In the two-photon case, photopolymerization occurs at the intersection of two scanning laser beams, although other configurations use a single laser and different photoinitiator chemistries. Another distinction is the need to recoat, or apply a new layer of resin, in the vector scan and mask projection approaches, while in the two-photon approach, the part is fabricated below the resin surface, making recoating unnecessary. Approaches that avoid recoating are faster and less complicated.

In this chapter, we first introduce photopolymer materials, then present the vector scan SL machines, technologies, and processes. Mask projection approaches are presented and contrasted with the vector scan approach. Additional configurations, along with their applications, are presented at the end of the chapter. Advantages, disadvantages, and uniquenesses of each approach and technology are highlighted.

4.2 Photopolymerization Materials

Some background of UV photopolymers will be presented in this section that is common to all configurations of photopolymerization processes. Two sections on reaction rates and characterization methods conclude this section. Much of this material is from the Jacobs book [1] and from a Masters thesis from the early 2000s [2].

4.2.1 UV Curable Photopolymers

As mentioned, photopolymers were developed in the late 1960s. In addition to the applications mentioned in Sect. 4.1, they are used as photoresists in the microelectronics industry. This application has had a major impact on the development of epoxy-based photopolymers. Photoresists are essentially one-layer SL, but with critical requirements on accuracy and feature resolution.

Various types of radiation may be used to cure commercial photopolymers, including gamma rays, X-rays, electron beams, UV, and in some cases visible light, although UV and electron beam are the most prevalent. In AM, many of these radiation sources have been utilized in research, however only UV and visible light systems are utilized in commercial systems. In SL systems, for example, UV radiation is used exclusively although, in principle, other types could be used. In the SLA-250 from 3D Systems, a helium-cadmium (HeCd) laser is used with a wavelength of 325 nm. In contrast, the solid-state lasers used in the other SL models are Nd-YVO_4. In mask projection DMD-based systems, UV and visible-light radiation are used.

Thermoplastic polymers that are typically injection molded have a linear or branched molecular structure that allows them to melt and solidify repeatedly.

In contrast, SL photopolymers are cross-linked and, as a result, do not melt and exhibit much less creep and stress relaxation. Figure 4.2 shows the three polymer structures mentioned [3].

The first US patents describing SL resins were published in 1989 and 1990 [4, 5]. These resins were prepared from acrylates, which had high reactivity but typically produced weak parts due to the inaccuracy caused by shrinkage and curling. The acrylate-based resins typically could only be cured to 46% completion when the image was transferred through the laser [6]. When a fresh coating was put on the exposed layer, some radiation went through the new coating and initiated new photochemical reactions in the layer that was already partially cured. This layer was less susceptible to oxygen inhibition after it had been coated. The additional crosslinking on this layer caused extra shrinkage, which increased stresses in the layer, and caused curling that was observed either during or after the part fabrication process [7].

The first patents that prepared an epoxide composition for SL resins appeared in 1988 [8, 9] (Japanese). The epoxy resins produced more accurate, harder, and stronger parts than the acrylate resins. While the polymerization of acrylate compositions leads to 5–20% shrinkage, the ring opening polymerization of epoxy compositions only leads to a shrinkage of 1–2% [10]. This low level of shrinkage associated with epoxy chemistry contributes to excellent adhesion and reduced tendency for flexible substrates to curl during cure. Furthermore, the polymerization of the epoxy-based resins is not inhibited by atmospheric oxygen. This enables low photoinitiator concentrations, giving lower residual odor than acrylic formulations [11].

However, the epoxy resins have disadvantages of slow photospeed and brittleness of the cured parts. The addition of some acrylate to epoxy resins is required to rapidly build part strength so that they will have enough integrity to be handled without distortion during fabrication. The acrylates are also useful to reduce the

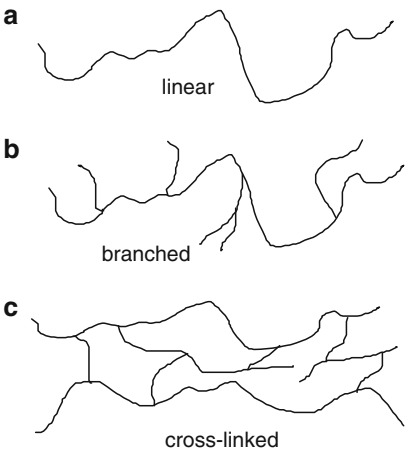

Fig. 4.2 Schematics of polymer types

brittleness of the epoxy parts [7]. Another disadvantage of epoxy resins is their sensitivity to humidity, which can inhibit polymerization [11].

As a result, most SL resins commercially available today are epoxides with some acrylate content. It is necessary to have both materials present in the same formulation to combine the advantages of both curing types. The improvement in accuracy resulting from the use of hybrid resins has given SL a tremendous boost.

4.2.2 Overview of Photopolymer Chemistry

SL photopolymers are composed of several types of ingredients: photoinitiators, reactive diluents, flexibilizers, stabilizers, and liquid monomers. Broadly speaking, when UV radiation impinges on SL resin, the photoinitiators undergo a chemical transformation and become "reactive" with the liquid monomers. A "reactive" photoinitiator reacts with a monomer molecule to start a polymer chain. Subsequent reactions occur to build polymer chains and then to cross-link – creation of strong covalent bonds between polymer chains. Polymerization is the term used to describe the process of linking small molecules (monomers) into larger molecules (polymers) composed of many monomer units [1]. Two main types of photopolymer chemistry are commercially evident:

- Free-radical photopolymerization – acrylate
- Cationic photopolymerization – epoxy and vinylether

The molecular structures of these types of photopolymers are shown in Fig. 4.5. Symbols C and H denote carbon and hydrogen atoms, respectively, while R denotes a molecular group which typically consists of one or more vinyl groups. A vinyl group is a molecular structure with a carbon–carbon double bond. It is these vinyl groups in the R structures that enable photopolymers to become cross-linked.

Free-radical photopolymerization was the first type that was commercially developed. Such SL resins were acrylates. Acrylates form long polymer chains once the photoinitiator becomes "reactive," building the molecule linearly by adding monomer segments. Cross-linking typically happens after the polymer chains grow enough so that they become close to one another. Acrylate photopolymers exhibit high photospeed (react quickly when exposed to UV radiation), but have a number of disadvantages including significant shrinkage and a tendency to warp and curl. As a result, they are rarely used now without epoxy or other photopolymer elements.

The most common cationic photopolymers are epoxies, although vinylethers are also commercially available. Epoxy monomers have rings, as shown in Fig. 4.3. When reacted, these rings open, resulting in sites for other chemical bonds. Ring-opening is known to impart minimal volume change on reaction, because the number and types of chemical bonds are essentially identical before and after reaction [12]. As a result, epoxy SL resins typically have much smaller shrinkages

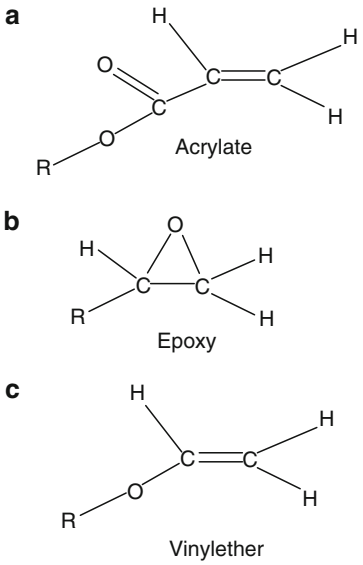

Fig. 4.3 Molecular structure of SL monomers

P-I → *-I•* (free radical formation)
I• + *M* → *I-M•* (initiation)
I-M• → → *I-M-M-M-M…-M•* (propagation)
→ *I-M-M-M-M…-M-I* (termination)

Fig. 4.4 Free-radical polymerization process

and much less tendency to warp and curl. Almost all commercially available SL resins have significant amounts of epoxies.

Polymerization of SL monomers is an exothermic reaction, with heats of reaction around 85 kJ/mol for an example acrylate monomer. Despite high heats of reaction, a catalyst is necessary to initiate the reaction. As described earlier, a photoinitiator acts as the catalyst.

Schematically, the free radical-initiated polymerization process can be illustrated as shown in Fig. 4.4 [1]. On average, for every two photons (from the laser), one radical will be produced. That radical can easily lead to the polymerization of over 1,000 monomers, as shown in the intermediate steps of the process, called propagation. In general, longer polymer molecules are preferred, yielding higher molecular weights. This indicates a more complete reaction. In Fig. 4.4, the *P–I* term indicates a photoinitiator, the $-I^{\bullet}$ symbol is a free radical, and *M* in a monomer.

Polymerization terminates from one of three causes, recombination, disproportionation, or occlusion. Recombination occurs when two polymer chains merge by

joining two radicals. Disproportionation involves essentially the cancelation of one radical by another, without joining. Occlusion occurs when free radicals become "trapped" within a solidified polymer, meaning that reaction sites remain available, but are prevented from reacting with other monomers or polymers by the limited mobility within the polymer network. These occluded sites will most certainly react eventually, but not with another polymer chain or monomer. Instead, they will react with oxygen or another reactive species that diffuses into the occluded region. This may be a cause of aging or other changes in mechanical properties of cured parts, which should be a topic of future research.

Cationic photopolymerization shares the same broad structure as free-radical polymerization, where a photoinitiator generates a cation as a result of laser energy, the cation reacts with a monomer, propagation occurs to generate a polymer, and a termination process completes the reaction. A typical catalyst for a cationic polymerization is a Lewis Acid, such as BF_3 [13]. Initially, cationic photopolymerization received little attention, but that has changed during the 1990s due to advances in the microelectronics industry, as well as interest in SL technology. We will not investigate the specifics of cationic reactions here, but will note that the ring-opening reaction mechanism of epoxy monomers is similar to radical propagation in acrylates.

4.2.3 Resin Formulations and Reaction Mechanisms

Basic raw materials such as polyols, epoxides, (meth) acrylic acids and their esters, diisocyanates etc. are used to produce the monomers and oligomers used for radiation curing. Most of the monomers are multifunctional monomers (MFM) or polyol polyacrylates which give a crosslinking polymerization. The main chemical families of oligomers are polyester acrylate (PEA), epoxy acrylates (EA), urethane acrylates (UA), amino acrylates (used as photoaccelerator in the photoinitiator system), and cycloaliphatic epoxies [11].

Resin suppliers create ready-to-use formulations by mixing the oligomers and monomers with a photoinitiator, as well as other materials to affect reaction rates and part properties. In practice, photosensitizers are often used in combination with the photoinitiator to shift the absorption toward longer wavelengths. In addition, supporting materials may be mixed with the initiator to achieve improved solubility in the formulation. Furthermore, mixtures of different types of photoinitiators may also be employed for a given application. Thus, photoinitiating systems are, in practice, often highly elaborate mixtures of various compounds which provide optimum performance for specific applications [10].

Other additives facilitate the application process and achieve products of good properties. A reactive diluent, for example, is usually added to adjust the viscosity of the mixtures to an acceptable level for application [14]; it also participates in the polymerization reaction.

4.2.3.1 Photoinitiator System

The role of the photoinitiator is to convert the physical energy of the incident light into chemical energy in the form of reactive intermediates. The photoinitiator must exhibit a strong absorption at the laser emission wavelength, and undergo a fast photolysis to generate the initiating species with a great quantum yield [15]. The reactive intermediates are either radicals capable of adding to vinylic or acrylic double bonds, thereby initiating radical polymerization, or reactive cationic species which can initiate polymerization reactions among epoxy molecules [10].

The free-radical polymerization process was outlined in Fig. 4.4, with the formation of free radicals as the first step. In the typical case in SL, radical photoinitiator systems include compounds that undergo unimolecular bond cleavage upon irradiation. This class includes aromatic carbonyl compounds that are known to undergo a homolytic C–C bond scission upon UV exposure [16]. The benzoyl radical is the major initiating species, while the other fragment may, in some cases, also contribute to the initiation. The most efficient photoinitiators include benzoin ether derivatives, benzyl ketals, hydroxyalkylphenones, α-amino ketones, and acylphosphine oxides [16, 17]. The Irgacure family of radical photoinitiators from Ciba Specialty Chemicals is commonly used in SL.

While photoinitiated free-radical polymerizations have been investigated for more than 60 years, the corresponding photoinduced cationic polymerizations have received much less attention. The main reason for the slow development in this area was the lack of suitable photoinitiators capable of efficiently inducing cationic polymerization [18]. Beginning in 1965, with the earliest work on diazonium salt initiators, this situation has markedly changed. The discovery in the 1970s of onium salts or organo-metallic compounds with excellent photoresponse and high efficiency has initiated the very rapid and promising development of cationic photopolymerization, and made possible the concurrent radical and cationic reaction in hybrid systems [19]. Excellent reviews have been published in this field [10, 18, 20–23]. The most important cationic photoinitiators are the onium salts, particularly the triarylsulphonium and diaryliodonium salts. Examples of the cationic photoinitiator are triaryl sulfonium hexafluorophosphate solutions in propylene carbonate such as Degacure KI 85 (Degussa), SP-55 (Asahi Denka), Sarcat KI-85 (Sartomer), and 53,113-8 (Aldrich), or mixtures of sulphonium salts such as SR-1010 (Sartomer, currently unavailable), UVI 6976 (B-V), and UVI 6992 (B-VI) (Dow).

Initiation of cationic polymerization takes place from not only the primary products of the photolysis of triarylsulphonium salts but also from secondary products of the reaction of those reactive species with solvents, monomers, or even other photolysis species. Probably the most ubiquitous species present is the protonic acid derived from the anion of the original salt. Undoubtedly, the largest portion of the initiating activity in cationic polymerization by photolysis of triarylsulphonium salts is due to protonic acids [18].

4.2.3.2 Monomer Formulations

The monomer formulations presented here are from a set of patents from the mid to late 1990s. Both di-functional and higher functionality monomers are used typically in SL resins. Poly(meth)acrylates may be tri-, pentafunctional monomeric or oligomeric aliphatic, cycloaliphatic or aromatic (meth)acrylates, or polyfunctional urethane (meth)acrylates [24–27]. One specific compound in the Huntsman SL-7510 resin includes the dipentaerythritol monohydroxy penta(meth)acrylates [26], such as Dipentaerythritol Pentaacrylate (SR-399, Sartomer).

The cationically curable epoxy resins may have an aliphatic, aromatic, cycloaliphatic, araliphatic, or heterocyclic structure; they on average possess more than one epoxide group (oxirane ring) in the molecule and comprise epoxide groups as side groups, or those groups form part of an alicyclic or heterocyclic ring system. Examples of epoxy resins of this type are also given by these patents such as polyglycidyl esters or ethers, poly(N or S-glycidyl) compounds, and epoxide compounds in which the epoxide groups form part of an alicyclic or heterocyclic ring system. One specific composition includes at least 50% by weight of a cycloaliphatic diepoxide [26] such as bis(2,3-epoxycyclopentyl) ether (formula A-I), 3,4-epoxycyclohexyl-methyl 3,4-epoxycyclohexanecarboxylate (A-II), dicyclopentadiene diepoxide (A-III), and bis-(3,4-epoxycyclohexylmethyl) adipate (A-IV).

Additional insight into compositions can be gained by investigating the patent literature further.

4.2.3.3 Interpenetrating Polymer Network Formation

As described earlier, acrylates polymerize radically, while epoxides cationically polymerize to form their respective polymer networks. In the presence of each other during the curing process, an interpenetrating polymer network (IPN) is finally obtained [28, 29]. An IPN can be defined as a combination of two polymers in network form, at least one of which is synthesized and/or crosslinked in the immediate presence of the other [30]. It is therefore a special class of polymer blends in which both polymers generally are in network form [30–32], and which is originally generated by the concurrent reactions instead of by a simple mechanical mixing process. In addition, it is a polymer blend rather than a copolymer that is generated from the hybrid curing [33], which indicates that acrylate and epoxy monomers undergo independent polymerization instead of copolymerization. However, in special cases, copolymerization can occur, thus leading to a chemical bonding of the two networks [34].

It is likely that in typical SL resins, the acrylate and epoxide react independently. Interestingly, however, these two monomers definitely affect each other physically during the curing process. The reaction of acrylate will enhance the photospeed

and reduce the energy requirement of the epoxy reaction. Also, the presence of acrylate monomer may decrease the inhibitory effect of humidity on the epoxy polymerization. On the other hand, the epoxy monomer acts as a plasticizer during the early polymerization of the acrylate monomer where the acrylate forms a network while the epoxy is still at liquid stage [31]. This plasticizing effect, by increasing molecular mobility, favors the chain propagation reaction [35]. As a result, the acrylate polymerizes more extensively in the presence of epoxy than in the neat acrylate monomer. Furthermore, the reduced sensitivity of acrylate to oxygen in the hybrid system than in the neat composition may be due to the simultaneous polymerization of the epoxide which makes the viscosity rise, thus slowing down the diffusion of atmospheric oxygen into the coating [31].

In addition, it has been shown [31] that the acrylate/epoxide hybrid system requires a shorter exposure to be cured than either of the two monomers taken separately. It might be due to the plasticizing effect of epoxy monomer and the contribution of acrylate monomer to the photospeed of the epoxy polymerization. The two monomers benefit from each other by a synergistic effect.

It should be noted that if the concentration of the radical photoinitiator was decreased so that the two polymer networks were generated simultaneously, the plasticizing effect of the epoxy monomer would become less pronounced. As a result, it would be more difficult to achieve complete polymerization of the acrylate monomer and thus require longer exposure time.

Although the acrylate/epoxy hybrid system proceeds via a heterogeneous mechanism, the resultant product (IPN) seems to be a uniphase component [36]. The properties appear to be extended rather than compromised [31, 34]. The optimal properties of IPNs for specific applications can be obtained by selecting two appropriate components and adjusting their proportions [34]. For example, increasing the acrylate content increases the cure speed but decreases the adhesion characteristics, while increasing the epoxy content reduces the shrinkage of curing and improves the adhesion, but decreases the cure speed [36].

4.3 Reaction Rates

As is evident, the photopolymerization reaction in SL resins is very complex. To date, no one has published an analytical photopolymerization model that describes reaction results and reaction rates. However, qualitative understanding of reaction rates is straightforward for simple formulations. Broadly speaking, reaction rates for photopolymers are controlled by concentrations of photoinitiators [I] and monomers [M]. The rate of polymerization is the rate of monomer consumption, which can be shown as [3]:

$$R_p = -d[M]/dt \ \alpha [M] \ (k[I])^{1/2} \tag{4.1}$$

where k = constant that is a function of radical generation efficiency, rate of radical initiation, and rate of radical termination. Hence, the polymerization rate is proportional to the concentration of monomer, but is only proportional to the square-root of initiator concentration.

Using similar reasoning, it can be shown that the average molecular weight of polymers is the ratio of the rate of propagation and the rate of initiation. This average weight is called the kinetic average chain length, v_o, and is given in (4.2):

$$v_o = R_p/R_i \ \alpha \ [M]/[I]^{1/2} \tag{4.2}$$

where R_i is the rate of initiation of macromonomers.

Equations (4.1) and (4.2) have important consequences for the SL process. The higher the rate of polymerization, the faster parts can be built. Since SL resins are predominantly composed of monomers, the monomer concentration cannot be changed much. Hence, the only other direct method for controlling the polymerization rate and the kinetic average chain length is through the concentration of initiator. However, (4.1) and (4.2) indicate a tradeoff between these characteristics. Doubling the initiator concentration only increases the polymerization rate by a factor of 1.4, but reduces the molecular weight of resulting polymers by the same amount. Strictly speaking, this analysis is more appropriate for acrylate resins, since epoxies continue to react after laser exposure, so (4.2) does not apply well for epoxies. However, reaction of epoxies is still limited, so it can be concluded that a trade-off does exist between polymerization rate and molecular weight for epoxy resins.

4.4 Vector Scan SL

A brief introduction to the vector scan-based (point-wise) SL process and SL systems from 3D Systems will be given here.

4.4.1 SL Process Overview

SL creates solid parts by selectively solidifying a liquid photopolymer resin using an UV laser. As with many other AM processes, the physical parts are manufactured by fabricating cross-sectional contours, or slices, one on top of another. These slices are created by tracing 2D contours of a CAD model in a vat of photopolymer resin with a laser. The part being built rests on a platform that is dipped into the vat of resin, as shown schematically in Fig. 4.1a. After each slice is created, the platform is lowered, the surface of the vat is recoated, then the laser starts to trace the next slice of the CAD model, building the prototype from the bottom up. A more complete description of the SL process may be found in [12]. The creation of the part requires a number of key steps: input data, part preparation, layer preparation, and finally laser scanning of the two-dimensional cross-sectional

slices. The input data consists of a STL created from a CAD file or reverse engineering data. Part preparation is the phase at which the operator specifies support structures, to hold each cross section in place while the part builds, and provides values for machine parameters. These parameters control how the prototype is fabricated in the SL machine. Layer preparation is the phase in which the STL model is divided into a series of slices, as defined by the part preparation phase, and translated by software algorithms into a machine language. This information is then used to drive the SL machine and fabricate the prototype. The laser scanning of the part is the phase that actually solidifies each slice in the SL machine.

After building the part, the part must be cleaned, post-cured, and finished. During either the cleaning and finishing phase, the SL machine operator may remove support structures. During finishing, the operator may spend considerable time sanding and filing the part to provide the desired surface finishes.

4.4.2 SL Machines

At present (2009), 3D Systems is the predominant manufacturer of SL machines in the world, although several other companies in Japan and elsewhere in Asia also market SL machines. Fockele & Schwarze in Germany produces a micro-SL technology, although they only sell design and manufacturing services. Several Japanese companies produce or produced machines, including Denken Engineering, CMET (Mitsubishi), Sony, Meiko Corp., Mitsui Zosen, and Teijin Seiki (license from Dupont).

A schematic of a typical SL machine was illustrated in Fig. 4.1a, which shows the main subsystems, including the laser and optics, the platform and elevator, the vat and resin-handling subsystem, and the recoater. The machine subsystem hierarchy is given in Fig. 4.5. Note that the five main subsystems are: recoating system, platform system, vat system, laser and optics system, and control system.

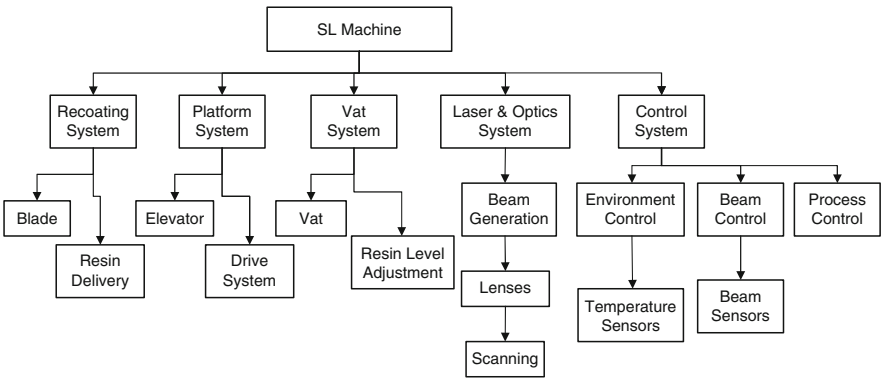

Fig. 4.5 Subsystems for SL technology

Typically, recoating is done using a shallow dip and recoater blade sweeping. Recoating issues are discussed in [37]. The process can be described as follows:

- After a layer has been cured the platform dips down by a layer thickness.
- The recoater blade slides over the whole build depositing a new layer of resin and smoothing the surface of the vat.

A common recoater blade type is the zephyr blade, which is a hollow blade that is filled with resin. A vacuum system pulls resin into the blade from the vat. As the blade translates over the vat to perform recoating, resin is deposited in regions where the previous part cross section was built. When the blade encounters a region in the vat without resin, the resin falls into this region since its weight is stronger than the vacuum force. Blade alignment is critical to avoid "blade crashes," when the blade hits the part being built and often delaminates the previous layer. The blade gap (distance between the bottom of the blade and the resin surface) and speed are important variables under user control.

The platform system consists of a build platform that supports the part being built and an elevator that lowers and raises the platform. The elevator is driven by a lead-screw. The vat system is simply the vat that holds the resin, combined with a level adjustment device, and usually an automated refill capability.

The optics system includes a laser, focusing and adjustment optics, and two galvanometers that scan the laser beam across the surface of the vat. Modern SL machines have solid-state lasers that have more stable characteristics than their predecessors, various gas lasers. SL machines from 3D Systems have Nd-YVO_4 lasers that output radiation at about 1,062 nm wavelength (near infrared). Additional optical devices triple the frequency to 354 nm, in the UV range. These lasers have relatively low power, in the range of 0.1–1 W, compared with lasers used in other AM and material processing applications.

The control system consists of three main subsystems. First, a process controller controls the sequence of machine operations. Typically, this involves executing the sequence of operations that are described in the build file that was prepared for a specific part or set of parts. Commands are sent to the various subsystems to actuate the recoating blade, to adjust resin level or changing the vat height, or to activate the beam controller. Sensors are used to detect resin height and to detect forces on the recoater blade to detect blade crashes. Second, the beam controller converts operation descriptions into actions that adjust beam spot size, focus depth, and scan speed, with some sensors providing feedback. Third, the environment controller adjusts resin vat temperature and, depending on machine model, adjusts environment temperature and humidity.

Two of the main advantages of SL technology over other AM technologies are part accuracy and surface finish, in combination with moderate mechanical properties. These characteristics led to the widespread usage of SL parts as form, fit, and, to a lesser extent, functional prototypes. Typical dimensional accuracies for SL machines are often quoted as a ratio of an error per unit length. For example, accuracy of a SLA-250 is typically quoted as 0.002 in./in. [38]. Modern SL machines are somewhat more accurate. Surface finish of SL parts ranges from

submicron Ra for upfacing surfaces to over 100 μm Ra for surfaces at slanted angles [39].

The current commercial SL product line from 3D Systems consists of two families of models: the SLA Viper Si2, and the iPro SLA Centers (iPro 9000XL, iPro 9000, and iPro 8000). Some of these machines are summarized in Table 4.1 [40]. Both the Viper Si2 and the iPro models have dual laser spot size capabilities. In the Viper Si2, a "high resolution" mode is available that provides a spot size of about 80 μm in diameter, useful for building small parts with fine features. In the iPro machines, in contrast, the machine automatically switches between the "normal" beam of 0.13 mm diameter for borders and fills and the "wide" beam of 0.76 mm diameter for hatch vectors (filling in large areas). The wide beam enables much faster builds. The iPro line replaces other

Table 4.1 Selected SL Systems (photos courtesy of 3D Systems, Inc.)

iPro 9000XL SLA Center	
Laser Type:	Solid state frequency tripled Nd:$YV0_4$
Wavelength:	354.7 nm
Power at vat @ 5000 hrs:	1450 mW
Recoating System	
Process:	Zephyr^{TM} Recoater
Layer Thickness Min:	0.05 mm (0.002 in)
Layer Thickness Max:	0.15 mm (0.006 in)
Optical & Scanning	
Beam diameter (@ 1/e2):	0.13 mm (borders) 0.76 (large hatch)
Drawing speed:	3.5 m/sec (borders) 25 m/sec (hatch)
Maximum part weight:	150 kg (330 lb)
Vat: Max. build envelope, Capacity	650x350x300 (39.1 gal) 650x750x50 (25.1 gal) 650x750x275 (71.9 gal) 650x750x550 (109 gal) 1500x750x550
iPro 8000 SLA Center	
Specification are the same as the iPro 9000XL, except	
Maximum part weight:	75 kg (165 lb)
Vat: Max. build envelope, Capacity	650x350x300 (39.1 gal) 650x750x50 (25.1 gal) 650x750x275 (71.9 gal) 650x750x550 (109 gal)
SLA Viper Si2	
Laser Type:	Solid State Nd:$YV0_4$
Wavelength:	354.7 nm
Power at vat:	100 mW

(*continued*)

Table 4.1 (continued)

Recoating System: Process:	Zephyr Recoater
Typical:	0.1 mm (0.004 in)*
Minimum:	0.05 mm (0.002 in)*
Optical & Scanning	
Beam diameter (@ 1/e2):	0.25 +/- 0.025 mm (0.01
Standard Mode	+/- 0.001 in)
High Resolution	0.075 +/- 0.015 mm (0.003 +/- 0.0005 in)
Part drawing speed:	5 mm/sec (0.2 in/sec)
Maximum part weight:	9.1 kg (20 lb)
Vat Capacity:	Volume:
Maximum build envelope:	250 x 250 x 200 mm XYZ (10 x 10 x 10 in)
	32.2 L (8.5 U.S. gal)
High Res. build envelope	125 x 125 x 250 mm (5 x 5 x 10 in)

machines, including the popular SLA-3500, SLA-5000, and SLA-7000 machines, as well as the SLA Viper Pro. Additionally, the SLA-250 was a very popular model that was discontinued in 2001 with the introduction of the Viper Si2 model.

4.5 SL Resin Curing Process

Background on SL materials and energy sources enables us to investigate the curing process of photopolymers in SL machines. We will begin with an investigation into the fundamental interactions of laser energy with photopolymer resins. Through the application of the Beer–Lambert law, the theoretical relationship between resin characteristics and exposure can be developed, which can be used to specify laser scan speeds. This understanding can then be applied to investigate mechanical properties of cured resins. From here, we will briefly investigate the ranges of size scales and time scales of relevance to the SL process. Much of this section is adapted from [1].

Nomenclature:

C_d = cure depth = depth of resin cure as a result of laser irradiation [mm]

D_p = depth of penetration of laser into a resin until a reduction in irradiance of $1/e$ is reached = key resin characteristic [mm]

E = exposure, possibly as a function of spatial coordinates [energy/unit area] [mJ/mm^2]

E_c = critical exposure = exposure at which resin solidification starts to occur [mJ/mm^2]

E_{max} = peak exposure of laser shining on the resin surface (center of laser spot) [mJ/mm^2]

$H(x,y,z)$ = irradiance (radiant power per unit area) at an arbitrary point in the resin = time derivative of $E(x,y,z)$.[W/mm^2]
P_L = output power of laser [W]
V_s = scan speed of laser [mm/s]
W_0 = radius of laser beam focused on the resin surface [mm]

4.5.1 Irradiance and Exposure

As a laser beam is scanned across the resin surface, it cures a line of resin to a depth that depends on many factors. However, it is also important to consider the width of the cured line as well as its profile. The shape of the cured line depends on resin characteristics, laser energy characteristics, and the scan speed. We will investigate the relationships among all of these factors in this subsection.

The first concept of interest here is *irradiance*, the radiant power of the laser per unit area, $H(x,y,z)$. As the laser scans a line, the radiant power is distributed over a finite area (beam spots are not infinitesimal). Figure 4.6 shows a laser scanning a line along the x-axis at a speed V_s [1]. Consider the z-axis oriented perpendicular to the resin surface and into the resin, and consider the origin such that the point of interest, p', has an x coordinate of 0. The irradiance at any point x,y,z in the resin is related to the irradiance at the surface, assuming that the resin absorbs radiation according to the Beer–Lambert Law. The general form of the irradiance equation for a Gaussian laser beam is given here as (4.3).

$$H(x,y,z) = H(x,y,0)\exp\left(-z/D_p\right) \tag{4.3}$$

From this relationship, we can understand the meaning of the penetration depth, D_p. Setting $z = D_p$, we get that the irradiance at a depth D_p is about 37% ($e^{-1} = 0.36788$) of the irradiance at the resin surface. Thus, D_p is the depth into the resin at which the irradiance is 37% of the irradiance at the surface. Furthermore, since we are assuming the Beer–Lambert Law holds, D_p is only a function of the resin.

Without loss of generality, we will assume that the laser scans along the x-axis from the origin to point b. Then, the irradiance at coordinate x along the scan line is given by

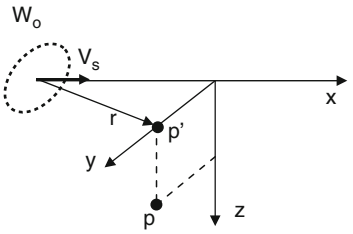

Fig. 4.6 Scan line of Gaussian laser

$$H(x, y, 0) = H(x, y) = H_0 e^{-2x^2/W_0^2} e^{-2y^2/W_0^2} \tag{4.4}$$

where $H_0 = H(0,0)$ when $x = 0$, and W_0 is the $1/e^2$ Gaussian half-width of the beam spot. Note that when $x = W_0$, $H(x,0) = H_0 e^{-2} = 0.13534 H_0$.

The maximum irradiance, H_0, occurs at the center of the beam spot ($x = 0$). H_0 can be determined by integrating the irradiance function over the area covered by the beam at any particular point in time. Changing from Cartesian to polar coordinates, the integral can be set equal to the laser power, P_L, as shown in (4.5).

$$P_L = \int_{r=0}^{r=\infty} H(r, 0)\, dA \tag{4.5}$$

When solved, H_o turns out to be a simple function of laser power and beam half-width, as in (4.6).

$$H_0 = \frac{2P_L}{\pi W_0^2} \tag{4.6}$$

As a result, the irradiance at any point x,y between $x = 0$ and $x = b$ is given by:

$$H(x, y) = \frac{2P_L}{\pi W_0^2} e^{-2x^2/W_0^2} e^{-2y^2/W_0^2} \tag{4.7}$$

However, we are interested in *exposure* at an arbitrary point, p, not irradiance, since exposure controls the extent of resin cure. Exposure is the energy per unit area; when exposure at a point in the resin vat exceeds a critical value, called E_c, we assume that resin cures. Exposure can be determined at point p by appropriately integrating (4.7) along the scan line, from time 0 to time t_b, when the laser reaches point b.

$$E(y, 0) = \int_{t=0}^{t=t_b} H[x(t), 0] dt \tag{4.8}$$

It is far more convenient to integrate over distance than over time. If we assume a constant laser scan velocity, then it is easy to substitute t for x, as in (4.9).

$$E(y, 0) = \frac{2P_L}{\pi V_s W_0^2} e^{-2y^2/W_0^2} \int_{x=0}^{x=b} e^{-2x^2/W_0^2} dx \tag{4.9}$$

The exponential term is difficult to integrate directly, so we will change the variable of integration. Define a variable of integration, v, as

$$v^2 \equiv \frac{2x^2}{W_0^2}$$

Then, take the square root of both sides, take the derivative, and rearrange to give

$$\mathrm{d}x = \frac{W_0}{\sqrt{2}}\mathrm{d}v$$

Due to the change of variables, it is also necessary to convert the integration limit to $b = \sqrt{2}/W_0 x_e$.

Several steps in the derivation will be skipped. After integration, the exposure received at a point x,y between $x = (0,b)$ can be computed as:

$$E(y,0) = \frac{P_\mathrm{L}}{\sqrt{2\pi}W_0 V_\mathrm{s}} \mathrm{e}^{-\frac{2y^2}{W_0^2}} [\mathrm{erf}(b)] \tag{4.10}$$

where erf(x) is the error function evaluated at x. erf(x) is 0 throughout almost the entire range of x between $-\infty$ and ∞. Only near $x = 0$ is it nonzero, which localizes the exposure within a narrow range around the scan vector. This makes sense since the laser beam is small and we expect that the energy received from the laser drops off quickly outside of its radius.

Equation (4.10) is not quite as easy to apply as a form of the exposure equation that results from assuming an infinitely long scan vector. If we make this assumption, then (5.9) becomes

$$E(y,0) = \frac{2P_\mathrm{L}}{\pi V_\mathrm{s} W_0^2} \mathrm{e}^{-2y^2/W_0^2} \int_{x=\infty}^{x=\infty} \mathrm{e}^{-2x^2/W_0^2} \mathrm{d}x$$

and after integration, exposure is given by

$$E(y,0) = \sqrt{\frac{2}{\pi}} \frac{P_\mathrm{L}}{W_0 V_\mathrm{s}} \mathrm{e}^{-2y^2/W_0^2} \tag{4.11}$$

Combining this with (4.3) yields the fundamental general exposure equation:

$$E(x,y,z) = \sqrt{\frac{2}{\pi}} \frac{P_\mathrm{L}}{W_0 V_\mathrm{s}} \mathrm{e}^{-2y^2/W_0^2} \mathrm{e}^{-z/D_\mathrm{p}} \tag{4.12}$$

4.5.2 Laser–Resin Interaction

In this subsection, we will utilize the irradiance and exposure relationships to determine the shape of a scanned vector line and its width. As we will see, the cross-sectional shape of a cured line becomes a parabola.

Starting with (4.12), the locus of points in the resin that is just at its gel point, where $E = E_c$, is denoted by y^* and z^*. Equation (4.12) can be rearranged, with y^*, z^*, and E_c substituted to give (4.13).

$$e^{2y^{*2}/W_0^2 + z^*/D_p} = \sqrt{\frac{2}{\pi}} \frac{P_L}{W_0 V_s E_c} \tag{4.13}$$

Taking natural logarithms of both sides yields

$$2\frac{y^{*2}}{W_0^2} + \frac{z^*}{D_p} = \ln\left[\sqrt{\frac{2}{\pi}} \frac{P_L}{W_0 V_s E_c}\right] \tag{4.14}$$

This is the equation of a parabolic cylinder in y^* and z^*, which can be seen more clearly in the following form,

$$ay^{*2} + bz^* = c \tag{4.15}$$

where a, b, and c are constants, immediately derivable from (4.14). Figure 4.7 illustrates the parabolic shape of a cured scan line.

To determine the maximum depth of cure, we can solve (4.14) for z^* and set $y^* = 0$, since the maximum cure depth will occur along the center of the scan vector. Cure depth, C_d, is given by

$$C_d = D_p \ln\left[\sqrt{\frac{2}{\pi}} \frac{P_L}{W_0 V_s E_c}\right] \tag{4.16}$$

As is probably intuitive, the width of a cured line of resin is the maximum at the resin surface; i.e., y_{max} occurs at $z = 0$. To determine line width, we start with the line shape function, (4.14). Setting $z = 0$ and letting line width, L_w, equal $2y_{max}$, the line width can be found:

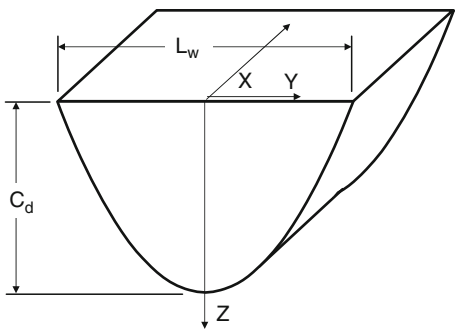

Fig. 4.7 Cured line showing parabolic shape, cure depth, and line width

$$L_w = W_0\sqrt{2C_d/D_p} \tag{4.17}$$

As a result, two important aspects become clear. First, line width is proportional to the beam spot size. Second, if a greater cure depth is desired, line width must increase, all else remaining the same. This becomes very important when performing line width compensation during process planning.

The final concept to be presented in this subsection is fundamental to commercial SL. It is the *working curve*, which relates exposure to cure depth, and includes the two key resin constants, D_p and E_c. At the resin surface and in the center of the scan line:

$$E(0,0) \equiv E_{max} = \sqrt{\frac{2}{\pi}}\frac{P_L}{W_0 V_s} \tag{4.18}$$

which is most of the expression within the logarithm term in (4.16). Substituting (4.18) into (4.16) yields the working curve equation:

$$C_d = D_p \ln\left(\frac{E_{max}}{E_c}\right) \tag{4.19}$$

In summary, a laser of power P_L scans across the resin surface at some speed V_s solidifying resin to a depth C_d, the cure depth, assuming that the total energy incident along the scan vector exceeds a critical value called the critical exposure, E_c. If the laser scans too quickly, no polymerization reaction takes place; i.e., exposure E is less than E_c. E_c is assumed to be a characteristic quantity of a particular resin.

An example working curve is shown in Fig. 4.8, where measured cure depths at a given exposure are indicated by "*." The working curve equation, (4.19), has several major properties [1]:

1. The cure depth is proportional to the natural logarithm of the maximum exposure on the centerline of a scanned laser beam.
2. A semilog plot of C_d vs. E_{max} should be a straight line. This plot is known as the *working curve* for a given resin.
3. The slope of the working curve is precisely D_p at the laser wavelength being used to generate the working curve.
4. The x-axis intercept of the working curve is E_c, the critical exposure of the resin at that wavelength. Theoretically, the cure depth is 0 at E_c, but this does indicate the gel point of the resin.
5. Since D_p and E_c are purely resin parameters, the slope and intercept of the working curve are independent of laser power.

In practice, various E_{max} values can be generated easily by varying the laser scan speed, as indicated by (4.19).

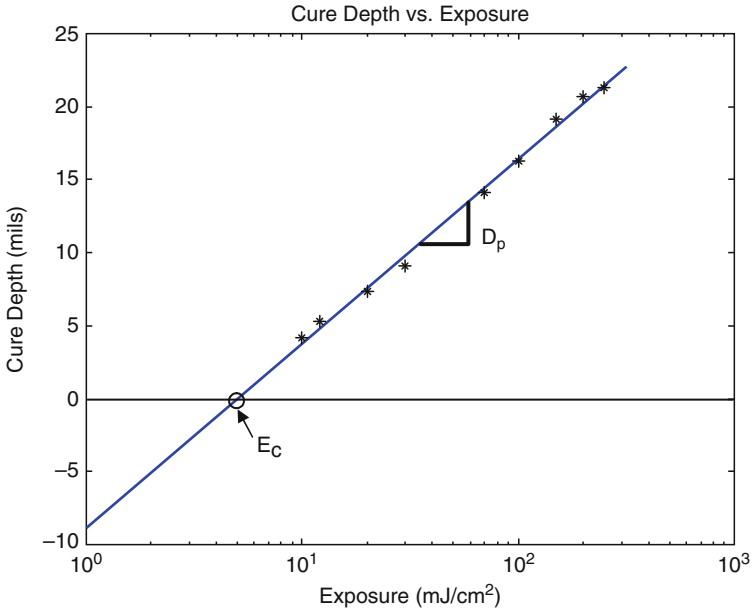

Fig. 4.8 Resin "working curve" of cure depth vs. exposure

4.5.3 Photospeed

Photospeed is typically used as an intuitive approximation of SL photosensitivity. But it is useful in that it relates to the speed at which the laser can be scanned across the polymer surface to give a specified cure depth. The faster the laser can be scanned to give a desired cure depth, the higher the photospeed. Photospeed is a characteristic of the resin and does not depend upon the specifics of the laser or optics subsystems. In particular, photospeed is indicated by the resin constants E_c and D_p.

To determine scan velocity for a desired cure depth, it is straightforward to solve (4.16) for V_s. Recall that at the maximum cure depth, the exposure received equals the cure threshold, E_c. Scan velocity is given by (4.20).

$$V_s = \sqrt{\frac{2}{\pi}} \frac{P_L}{W_0 E_c} e^{-C_d/D_p} \tag{4.20}$$

This discussion can be related back to the working curve. Both E_c and D_p must be determined experimentally. 3D Systems has developed a procedure called the WINDOWPANE procedure for finding E_c and D_p values [41]. The cure depth, C_d, can be measured directly from specimens built on an SL machine that are one layer thickness in depth. The WINDOWPANE procedure uses a specific part shape, but the principle is simply to build a part with different amounts of laser exposure in

different places in the part. By measuring the part thickness, C_d, and correlating that with the exposure values, a "working curve" can easily be plotted. Note that (4.19) is log-linear. Hence, C_d is plotted linearly vs. the logarithm of exposure to generate a working curve.

So how is exposure varied? Exposure is varied by simply using different scan velocities in different regions of the WINDOWPANE part. The different scan velocities will result in different cure depths. In practice, (4.20) is very useful since we want to directly control cure depth, and want to determine how fast to scan the laser to give that cure depth. Of course, for the WINDOWPANE experiment, it is more useful to use (4.16) or (4.19).

4.5.4 Time Scales

It is interesting to investigate the time scales at which SL operates. On the short end of the time scale, the time it takes for a photon of laser light to traverse a photopolymer layer is about a picosecond (10^{-12} s). Photon absorption by the photoinitiator and the generation of free radicals or cations occur at about the same time frame. A measure of photopolymer reaction speed is the kinetic reaction rates, t_k, which are typically several microseconds.

The time it takes for the laser to scan past a particular point on the resin surface is related to the size of the laser beam. We will call this time the characteristic exposure time, t_e. Values of t_e are typically 50–2000 μs, depending on the scan speed (500–5000 mm/s). Laser exposure continues long after the onset of polymerization. Continued exposure generates more free radicals or cations and, presumably, generates these at points deeper in the photopolymer. During and after the laser beam traverses the point of interest, cross-linking occurs in the photopolymer.

The onset of measurable shrinkage, $t_{s,o}$, lags exposure by several orders of magnitude. This appears to be due to the rate of cross-linking, but for the epoxy-based resins, may have more complicated characteristics. Time at corresponding completion of shrinkage is denoted $t_{s,c}$. For the acrylate-based resins of the early 1990s, times for the onset and completion of shrinkage were typically 0.4–1 and 4–10 s, respectively. Recall that epoxies can take hours or days to polymerize. Since shrinkage lags exposure, this is clearly a phenomena that complicates the SL process. Shrinkage leads directly to accuracy problems, including deviation from nominal dimensions, warpage, and curl.

The final time dimension is that of scan time for a layer, denoted t_d, which typically spans 10–300 s. The time scales can be summarized as

$$t_t << t_k << t_e << t_{s,o} < t_{s,c} << t_d \tag{4.21}$$

As a result, characteristic times for the SL process span about 14 orders of magnitude.

4.6 SL Scan Patterns

4.6.1 Layer-Based Build Phenomena and Errors

Several phenomena should be noted since they are common to all radiation and layer-based AM processes. The most obvious phenomenon is discretization; e.g., a stack of layers causes "stair steps" on slanted or curved surfaces. So, the layer-wise nature of most AM processes causes edges of layers to be visible. Conventionally, commercial AM processes build parts in a "material safe" mode, meaning that the stair steps are on the outside of the CAD part surfaces. Technicians can sand or finish parts; the material they remove is outside of the desired part geometry. Other discretization examples are the set of laser scans or the pixels of a DMD. In most processes, individual laser scans or pixels are not visible on part surfaces, but in other processes such as Fused Deposition Modeling the individual filaments are noticeable.

As a laser scans a cross section, or a lamp illuminates a layer, the material solidifies and, as a result, shrinks. When resins photopolymerize, they shrink since the volume occupied by monomer molecules is larger than that of reacted polymer. Similarly, after powder melts, it cools and freezes, which reduces the volume of the material. When the current layer is processed, its shrinkage pulls on the previous layers, causing stresses to build up in the part. Typically, those stresses remain and are called residual stresses. Also, those stresses can cause part edges to curl upwards. Other warpage or part deformations can occur due to these residual stresses, as well.

The last phenomenon to be discussed is that of print-through errors. In photopolymerization processes, it is necessary to have the current layer cure into the previous layer. In powder bed fusion processes, the current layer needs to melt into the previous layer so that one solid part results, instead of a stack of disconnected solid layers. The extra energy that extends below the current layer results in thicker part sections. This extra thickness is called print-through error in SL and "bonus Z" in laser sintering. Most process planning systems compensate for print-through by giving users the option of skipping the first few layers of a part, which works well unless important features are contained within those layers.

These phenomena will be illustrated in this section through an investigation of scan patterns in SL.

4.6.2 WEAVE

Prior to the development of WEAVE, scan patterns were largely an ad hoc development. As a result, post-cure curl distortion was the major accuracy problem. The WEAVE scan pattern became available for use in late 1990, [1].

The development of WEAVE began with the observation that distortion in post-cured parts was proportional to the percent of uncured resin after removal from the SL vat. Another motivating factor was the observation that shrinkage lags exposure and that this time lag must be considered when planning the pattern of laser scans.

The key idea in WEAVE development was to separate the curing of the majority of a layer from the adherence of that layer to the previous layer. Additionally, to prevent laser scan lines from interfering with one another while each is shrinking, parallel scans were separated from one another by more than a line width.

The WEAVE style consists of two sets of parallel laser scans:

- First, parallel to the x-axis, spaced 1 mil (1 mil = 0.001 in. = 0.25 mm, which historically is a standard unit of measure in SL) apart, with a cure depth of 1 mil less than the layer thickness.
- Second, parallel to the y-axis, spaced 1 mil apart, again with a cure depth of 1 mil less than the layer thickness.

However, it is important to understand the relationships between cure depth and exposure. On the first pass, a certain cure depth is achieved, C_{d1}, based on an amount of exposure, E_{max1}. On the second pass, the same amount of exposure is provided and the cure depth increases to C_{d2}. A simple relationship can be derived among these quantities, as shown in (4.21).

$$C_{d2} = D_p \ln(2E_{max1}/E_c) \; = D_p \ln(2) + D_p \ln(E_{max1}/E_c) \tag{4.21}$$

$$C_{d2} = C_{d1} + D_p \ln(2) \tag{4.22}$$

It is the second pass that provides enough exposure to adhere the current layer to the previous one. The incremental cure depth caused by the second pass is just ln(2) D_p, or about $0.6931D_p$. This distance is always greater than 1 mil.

As mentioned, a major cause of post-cure distortion was the amount of uncured resin after scanning. The WEAVE build style cures about 99% of the resin at the vat surface and about 96% of the resin volume through the layer thickness. Compared with previous build styles, WEAVE provided far superior results in terms of eliminating curl and warpage. Figure 4.9 shows a typical WEAVE pattern, illustrating how WEAVE gets its name.

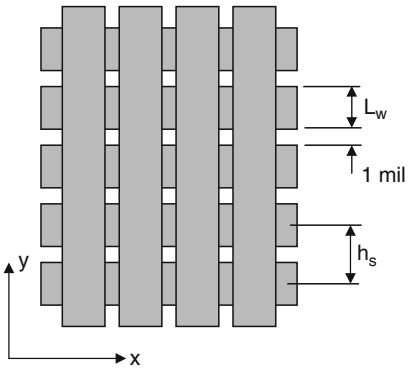

Fig. 4.9 WEAVE scan pattern

Even though WEAVE was a tremendous improvement, several flaws were observed with its usage. Corners were distorted on large flat surfaces, one of these corners always exhibited larger distortion, and it was always the same corner. Some microfissures occurred; on a flat plate with a hole, a macrofissure tangent to the hole would appear.

It was concluded that significant internal stresses developed within parts during part building, not only post-cure. As a result, improvements to WEAVE were investigated, leading to the development of STAR-WEAVE.

4.6.3 STAR-WEAVE

STAR-WEAVE was released in October 1991, roughly 1 year after WEAVE [1]. STAR-WEAVE addressed all of the known deficiencies of WEAVE and worked very well with the resins available at the time. WEAVE's deficiencies were traced to the consequences of two related phenomena: the presence of shrinkage and the lag of shrinkage relative to exposure. These phenomena led directly to the presence of large internal stresses in parts. STAR-WEAVE gets its name from the three main improvements from WEAVE:

1. Staggered hatch
2. Alternating sequence
3. Retracted hatch

Staggered hatch directly addresses the observed microfissures. Consider Fig. 4.10 which shows a cross-sectional view of the hatch vectors from two layers. In Fig. 4.10a, the hatch vectors in WEAVE form vertical "walls" that do not directly touch. In STAR-WEAVE, Fig. 4.10b, the hatch vectors are staggered such that they directly adhere to the layer below. This resulting overlap from one layer to the next eliminated microfissures and eliminated stress concentrations in the regions between vectors.

Upon close inspection, it became clear why the WEAVE scan pattern tended to cause internal stresses, particularly if a part had a large cross section. Consider a thin cross section, as shown in Fig. 4.11. The WEAVE pattern was set up to always

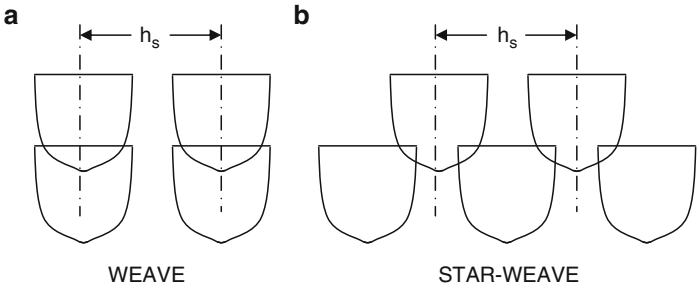

Fig. 4.10 Cross-sectional view of WEAVE and STAR-WEAVE patterns

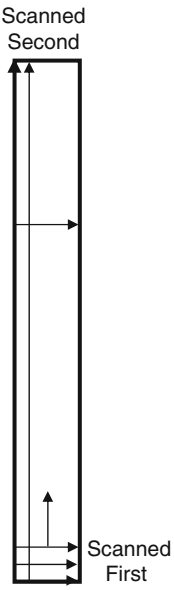

Fig. 4.11 WEAVE problem example

proceed in a certain manner. First, the *x*-axis vectors were drawn left to right, and front to back. Then, the *y*-axis vectors were drawn front to back and left to right. Consider what happens as the *y*-axis vectors are drawn and the fact that shrinkage lags exposure. As successive vectors are drawn, previous vectors are shrinking, but these vectors have adhered to the *x*-axis vectors and to the previous layer. In effect, the successive shrinkage of *y*-axis vectors causes a "wave" of shrinkage from left to right, effectively setting up significant internal stresses. These stresses cause curl.

Given this behavior, it is clear that square cross sections will have internal stresses, possibly without visible curl. However, if the part cannot curl, the stresses will remain and may result in warpage or other form errors.

With a better understanding of curing and shrinking behavior, the Alternating Sequence enhancement to building styles was introduced. This behavior can be alleviated to a large extent simply by varying the *x* and *y* scan patterns. There are two vector types: *x* and *y*. These types can be drawn left to right, right to left, front to back, and back to front. Looking at all combinations, eight different scan sequences are possible. As a part is being built, these eight scan sequences alternate, so that eight consecutive layers have different patterns, and this pattern is repeated every eight layers.

The good news is that internal stresses were reduced and the macrofissures disappeared. However, internal stresses were still evident. To alleviate the internal stresses to a greater extent, the final improvement in STAR-WEAVE was introduced, that of Retracted Hatch. It is important to realize that the border of a cross section is scanned first, then the hatch is scanned. As a result, the *x*-axis vectors adhere to both the left and right border vectors. When they shrink, they pull on the

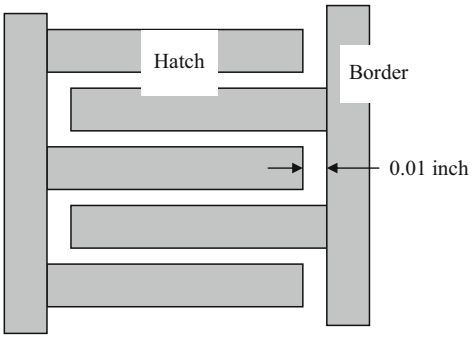

Fig. 4.12 Retracted hatch of the STAR-WEAVE pattern

borders, bending them toward one another, causing internal stresses. To alleviate this, alternating hatch vectors are retracted from the border, as shown in Fig. 4.12. This retracted hatch is performed for both the *x* and *y* vectors.

4.6.4 ACES Scan Pattern

With the development of epoxy-based photopolymers in 1992–1993, new scan patterns were needed to best adopt to their curing characteristics. ACES (Accurate, Clear, Epoxy, Solid) was the answer to these needs. ACES is not just a scan pattern, but is a family of build styles. The operative word in the ACES acronym is Accurate. ACES was mainly developed to provide yet another leap in part accuracy by overcoming deficiencies in STAR-WEAVE, most particularly, in percent of resin cured in the vat. Rather than achieving 96% solidification, ACES is typically capable of 98%, further reducing post-cure shrinkage and the associated internal stresses, curl, and warpage [12].

SL operators have a lot of control over the particular scan pattern used, along with several other process variables. For example, while WEAVE and STAR-WEAVE utilized 0.001 in. spacings between solidified lines, ACES allows the user to specify hatch spacing. Table 4.2 shows many of the process variables for the SLA-250 along with typical ranges of variable settings.

In Table 4.2, the first four variables are called scan variables since they control the scan pattern, while the remaining variables are recoat variables since they control how the vat and part are recoated. With this set of variables, the SL operator has a tremendous amount of control over the process; however, the number of variables can cause a lot of confusion since it is difficult to predict exactly how the part will behave as a result of changing a variable's value. To address this issue, 3D Systems provides nominal values for many of the variables as a function of layer thickness.

The fundamental premise behind ACES is that of curing more resin in a layer before bonding that layer to the previous one. This is accomplished by overlapping hatch vectors, rather than providing 0.001 in. spacing between hatch vectors. As a result, each point in a layer is exposed to laser radiation from multiple scans. Hence,

Table 4.2 ACES process variables for the SLA-250

Variable	Range
Layer thickness	0.002–0.008 in.
Hatch spacing	0.006–0.012 in.
Hatch overcure	(−0.003)–(+0.001) in.
Fill overcure	0.006–0.012 in.
Blade gap %	100–200
Sweep period	5–15 s
Z-Wait	0–20 s
Pre-Dip delay	0–20 s

it is necessary to consider these multiple scans when determining cure depth for a layer. ACES also makes use of two passes of scan vectors, one parallel to the x-axis and one parallel to the y-axis. In the first pass, the resin is cured to a depth 1 mil less than the desired layer thickess. Then on the second pass, the remaining resin is cured and the layer is bonded to the previous one.

As might be imagined, more scan vectors are necessary using the ACES scan pattern, compared with WEAVE and STAR-WEAVE.

The remaining presentation in this section is on the mathematical model of cure depth as a function of hatch spacing to provide insight into the cure behavior of ACES.

Consider Fig. 4.13 that shows multiple, overlapping scan lines with hatch spacing h_s. Also shown is the cure depth of each line, C_{d_0}, and the cure depth, C_{d_1}, of the entire scan pass. As we know from earlier, the relationship between exposure and cure depth is given by (4.23).

$$C_{d_0} = D_p \ln(E_{max}/E_c) \tag{4.23}$$

The challenge is to find an expression for cure depth of a scan pass when the scan vectors overlap. This can be accomplished by starting from the relationship describing the spatial distribution of exposure. From earlier, we know that:

$$E(y,0) = E_{max} e^{-\left(2y^2/W_0^2\right)} \tag{4.24}$$

Consider the progression of curing that results from many more scans in Fig. 4.13. If we consider a point P in the region of the central scan, we need to determine the number of scan vectors that provide significant exposure to P. Since the region of influence is proportional to beam spot size, the number of scans depends upon the beam size and the hatch spacing. Considering that the ratio of hatch spacing to beam half-width, W_0, is rarely less than 0.5 (i.e., h_s / $W_0 \geq 0.5$), then we can determine that point P receives about 99% of its exposure from a distance of 4 h_s or less. In other words, if we start at the center of a scan vector, at most, we need to consider 4 scans to the left and 4 scans to the right when determining cure depth.

In this case, we are only concerned with the variation of exposure with y, the dimension perpendicular to the scan direction.

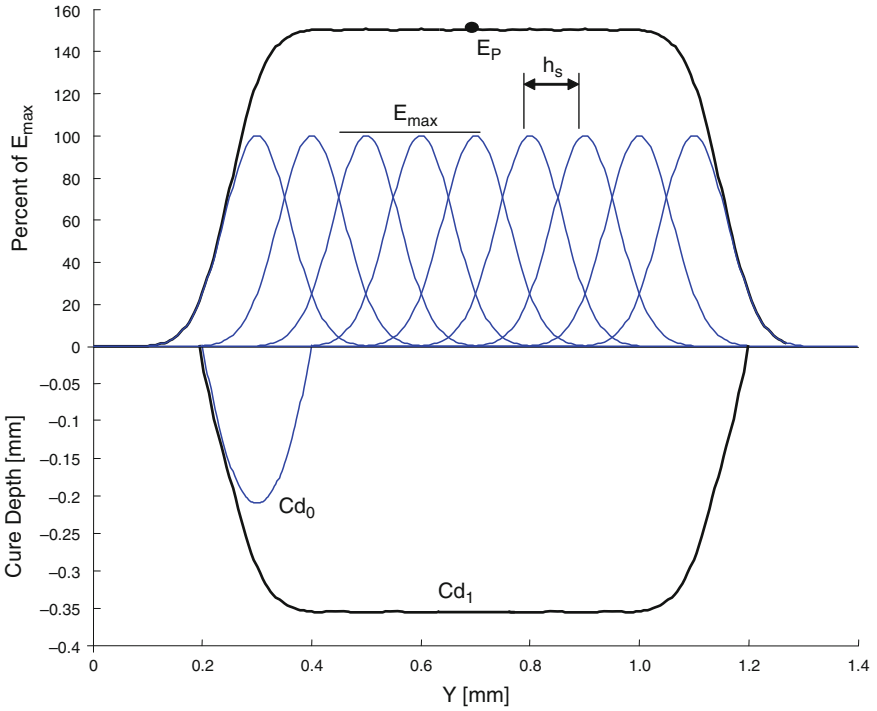

Fig. 4.13 Cure depth and exposure for the ACES scan pattern

Given that it is necessary to consider 9 scans, we know the various values of y in (4.24). We can consider that $y = nh_s$, and let n range from −4 to +4. Then, the total exposure received at a point P is the sum of the exposures received over those 9 scans, as shown in (4.25) and (4.26).

$$E_p = E_0 + \ 2E_1 + \ 2E_2 + \ 2E_3 + \ 2E_4 \tag{4.25}$$

where $E_n \equiv E(n\ h_s, 0) \ = E_{max} e^{-2(nh_s/W_0)^2}$

$$E_P = E_{max}\left[1 + 2e^{-2(h_s/W_0)^2} + 2e^{-8(h_s/W_0)^2} + 2e^{-18(h_s/W_0)^2} + 2e^{-32(h_s/W_0)^2}\right] \tag{4.26}$$

It is convenient to parameterize exposure vs. E_{max} against the ratio of hatch spacing vs. beam half-width. A simple rearrangement of (4.26) yields (4.27). A plot of (4.27) over the typical range of size ratios (h_s / W_0) is shown in Fig. 4.14.

$$\frac{E_P}{E_{max}} = 1 + \sum_{n=1}^{4} e^{-2(nh_s/W_0)^2} \tag{4.27}$$

We can now return to our initial objective of determining the cure depth for a single pass of overlapping scan vectors. Further, we can determine the increase in cure depth from a single scan to the entire layer. A cure depth for a single pass, C_{d_1}, with overlapping scans is a function of the total exposure given in (4.26). C_{d_1} is determined using (4.28).

$$C_{d_1} = D_{\mathrm{p}} \ln(E_{\mathrm{P}}/E_{\mathrm{c}}) \tag{4.28}$$

The cure depth increase is given by $C_{d_1} - C_{d_0}$ and can be determined using (4.29).

$$C_{d_1} - C_{d_0} = D_{\mathrm{p}} \ln(E_{\mathrm{P}}/E_{\max}) \tag{4.29}$$

As an example, consider that we desire a layer thickness to be 4 mils using a resin with a D_{p} of 5.8 mils. Assume further that the desired hatch spacing is 6 mils and the beam half-width is 5 mils, giving a size ratio of $h_{\mathrm{s}} / W_0 = 1.2$. On the first pass, the cure depth, C_{d_1}, should be $4 - 1 = 3$ mils. From (4.27), the exposure ratio can be determined to be 1.1123 (or see Fig. 4.14). The cure depth for a single scan vector can be determined by rearranging (4.29) to solve for C_{d_0}.

$$\begin{aligned} C_{d_0} &= C_{d_1} - D_{\mathrm{p}} \ln(E_{\mathrm{P}}/E_{\max}) \\ &= 3 \; - \; 5.8 \; * \ln(1.1123) \\ &= 2.383 \text{ mils} \end{aligned}$$

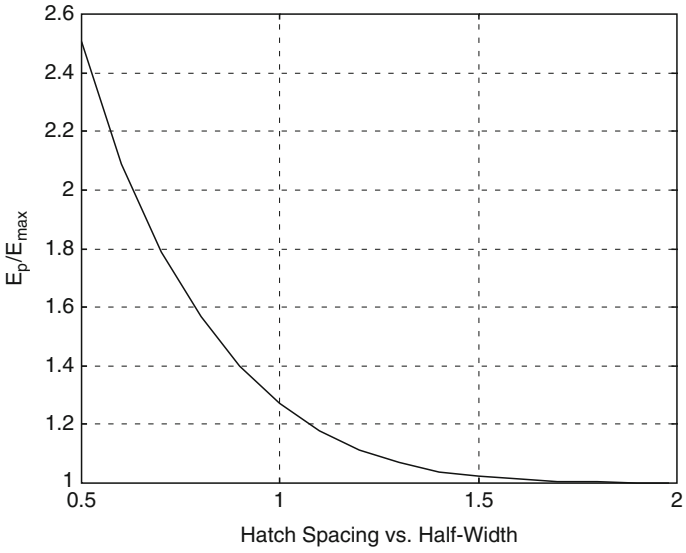

Fig. 4.14 Plot of (4.27): exposure ratios vs. size ratios

From this calculation, it is evident that the cure depth of a single scan vector is 1.6 mils less than the desired layer thickness. Rounding up, we say that the hatch overcure of this situation is −2 mils. Recall that the hatch overcure is one of the variables that can be adjusted by the SL machine operator.

This concludes the presentation of traditional vector scan SL. We now proceed to discuss micro-stereolithography and mask projection-based systems, where areas of the vat surface are illuminated simultaneously to define a part cross section.

4.7 Vector Scan Microstereolithography

Several processes were developed exclusively for microfabrication applications based on photopolymerization principles using both lasers and X rays as the energy source. These processes build complex shaped parts that are typically less than 1 mm in size. They are referred to as Microstereolithography (MSL), Integrated Hardened Stereolithography (IH), LIGA [42], Deep X-ray Lithography (DXRL), and other names. In this section, we will focus on those processes that utilize UV radiation to directly process photopolymer materials.

In contrast to convention SL, vector scan technologies for the micro-scale typically have moved the vat in x, y, and z directions, rather than scanning the laser beam. To focus a typical laser to spot sizes less than 20 μm requires the laser's focal length to be very short, causing difficulties for scanning the laser. For an SLA-250 with a 325 nm wavelength HeCd laser, the beam has a diameter of 0.33 mm and a divergence of 1.25 mrad as it exits the laser. It propagates 280 mm then encounters a diverging lens (focal length −25 mm) and a converging lens (focal length 100 mm) which is 85 mm away. Using simple thin-lens approximations, the distance from the converging lens to the focal point, where the laser reaches a spot size of 0.2 mm is 940 mm and its Rayleigh range is 72 mm. Hence, the focused laser spot is a long distance from the focusing optics and the Rayleigh range is long enough to enable a wide scanning region and a large build area.

In contrast, a typical calculation is presented here for a high resolution micro-SL system with a laser spot size of 10 μm. A 325 nm wavelength HeCd laser used in SL is included here to give the reader an idea of the challenge. The beam, as it exits the laser, has a diameter of 0.33 mm and a divergence of 1.25 mrad. It propagates 280 mm then encounters a diverging lens (focal length −25 mm) and a converging lens (focal length 36.55 mm). The distance from the converging lens to the focal point is 54.3 mm and its Rayleigh range is only 0.24 mm. It would be very difficult to scan this laser beam across a vat without severe spot distortions.

Scanning micro-SL systems have been presented in literature since 1993 with the introduction of the Integrated Hardening method of Ikuta and Hirowatari [43]. They used a laser spot focused to a 5-μm diameter and the resin vat is scanned underneath it to cure a layer. Examples of devices built with this method include tubes, manifolds, and springs and flexible microactuators [44] and fluid channels on silicon [45]. Takagi and Nakajima [46] have demonstrated the use of this technology for connecting MEMS gears together on a substrate. The artifact fabricated

using micro-SL can be used as a mold for subsequent electroplating followed by removal of the resin [47]. This method has been able to achieve sub-1 μm minimum feature size.

The following specifications of a typical point-wise Microstereolithography process have been presented in [48]:

- 5-μm spot size of the UV beam
- Positional accuracy is 0.25 μm (in the *x*–*y* directions) and 1.0 μm in the *z*-direction
- Minimum size of the unit of hardened polymer is 5 μm × 5 μm × 3 μm (in *x*, *y*, *z*)
- Maximum size of fabrication structure is 10 mm × 10 mm × 10 mm

The capability of building around inserted components has also been proposed for components such as ultrafiltration membranes and electrical conductors. Applications include fluid chips for protein synthesis [49] and bioanalysis [50]. The bioanalysis system was constructed with integrated valves and pumps that include a stacked modular design, 13 × 13 mm^2 and 3 mm thick, each of which has different fluid function. However, the full extent of integrated processing on silicon has not yet been demonstrated. The benefits of greater design flexibility and lower cost of fabrication may be realized in the future.

4.8 Mask Projection Photopolymerization Technologies and Processes

Technologies to project bitmaps onto a resin surface to cure a layer at a time were first developed in the early 1990s by researchers who wanted to develop special SL machines to fabricate microscale parts. Several groups in Japan and Europe pursued mask projection stereolithography (MPSL) technology at that time. The main advantage of mask projection methods is speed: since an entire part cross section can be cured at one time, it can be faster than scanning a laser beam. Dynamic masks can be realized by LCD screens, by spatial light modulators, or by DMDs, such as the Digital Light Processing (DLP™) chips manufactured by Texas Instruments [51].

4.8.1 Mask Projection SL Technology

MPSL systems have been realized by several groups around the world. Some of the earlier systems utilized LCD displays as their dynamic mask [52, 53], while another early system used a spatial light modulator [54]. The remaining systems all used DMDs as their dynamic masks [55–58]. These latest systems all use UV lamps as their radiation source, while others have used lamps in the visible range [55] or

lasers in the UV. A good overview of micro-SL technology, systems, and applications is the book by Varadan et al. [59].

MSL has been commercialized by MicroTEC GmbH, Germany. Although machines are not for sale, the company offers customer-specific services. The company has developed machines based on point-wise as well as layer-wise photopolymerization principles. Their Rapid Micro Product Development (RMPD) machines using a He–Cd laser enable construction of small parts layer-by-layer (as thin as 1 μm) with a high surface quality in the subnanometer range and with a feature definition of <10 μm.

A schematic and photograph of the MPSL system from Georgia Tech is shown in Fig. 4.15. Similar to conventional SL, the MPSL process starts with the CAD model of the part, which is then sliced at various heights. Each resulting slice cross section is stored as bitmaps to be displayed on the dynamic mask. UV radiation reflects off of the "on" micro-mirrors and is imaged onto the resin surface to cure a layer. In the system at Georgia Tech, a broadband UV lamp is the light source, a DMD is the dynamic mask, and an automated XYZ stage is used to translate the vat of resin in three dimensions. Standard SL resins are typically used, although other research groups formulate their own.

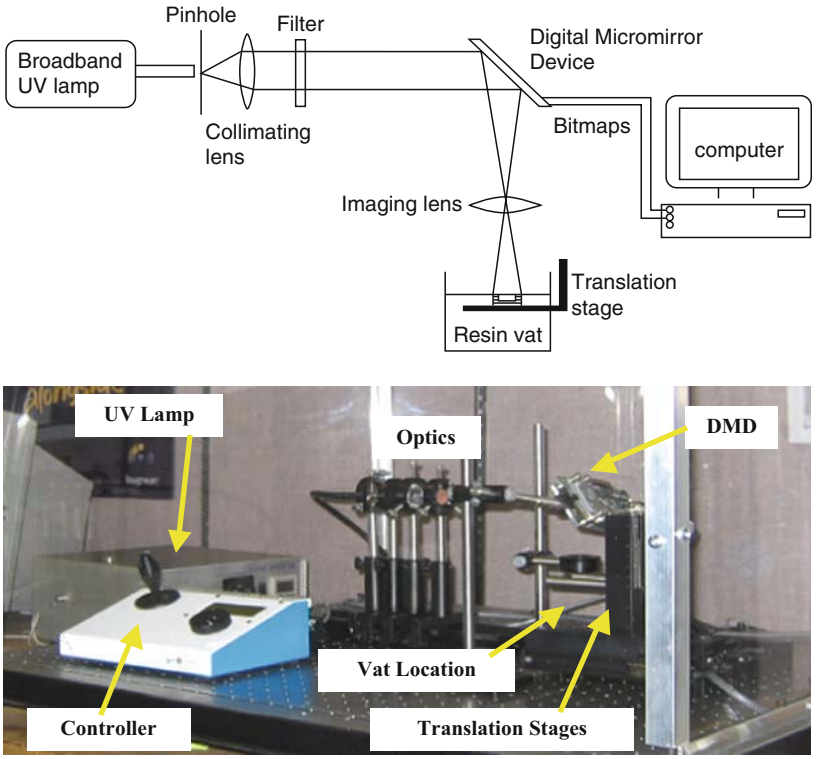

Fig. 4.15 Schematic and photo of mask projection stereolithography machine

4.8.2 Commercial MPSL Systems

Two companies market SL systems based on mask projection technology, EnvisionTec and 3D Systems.

EnvisionTEC first marketed their MPSL systems in 2003. They now have several lines of machines with various build envelopes and resolutions based on the MPSL process, including the Perfactory, Perfactory Desktop, Aureus, Xede/Xtreme, and Ultra. Variants of some of these models are available, including specialized Perfactory machines for dental restorations or for hearing aid shells. A photo of the Perfactory Standard machine is shown in Fig. 4.16 and its technical specifications are listed in Table 4.3.

Schematically, their machines are very similar to the Georgia Tech machine in Fig. 4.15 and utilize a lamp for illuminating the DMD and vat. However, several of their machine models have a very important difference: they build parts upside down and do not use a recoating mechanism. The vat is illuminated vertically upwards through a clear window. After the system irradiates a layer, the cured resin sticks to the window and cures into the previous layer. The build platform pulls away from the window at a slight angle to gently separate from the window. The advantage of this approach is threefold. First, no separate recoating mechanism is needed since gravity forces the resin to fill in the region between the cured part and the window. Second, the top vat surface being irradiated is a flat window, not a free surface, enabling more precise layers to be fabricated. Third, they have devised a

Fig. 4.16 EnvisionTEC Perfactory model

Table 4.3 Specifications on EnvisionTEC Perfactory Standard Zoom machine

Lens system		$f = 25$–45 mm
Build envelope	Standard	190 × 142 × 230 mm
	High resolution	120 × 90 × 230 mm
Pixel size	Standard	86–136 μm
	High resolution	43–68 μm
Layer thickness	25–150 mm	

build process that eliminates a regular vat. Instead, they have a supply on demand material feed system. The disadvantage is that small or fine features may be damaged when the cured layer is separated from the window.

3D Systems introduced their V-Flash machine in 2008, which utilizes MPSL technology and a novel material handling approach [60]. The V-Flash is intended to be an inexpensive prototyping machine (under $10,000) that is as easy to use as a typical home ink-jet printer. Its build envelope is 230 × 170 × 200 mm (9 × 7 × 8 in.). During operation, parts are built upside down. For each layer, a blade coats a layer of resin onto a film that spans the build chamber. The build platform slides down until the platform or the in-process part contacts the resin layer and film. A cartridge provides a supply of unused film for each layer. That layer is cured by the machine's "UV Imager," which consists of the MPSL technology. This process continues until the entire part is built. Some rinsing of the part is required, similar to SL, and support structures may have to be removed during the post-processing phase of part fabrication.

4.8.3 MPSL Modeling

Most of the research presented on MPSL technology is experimental. As in SL, it is possible to develop good predictive models of curing for MPSL systems. Broadly speaking, models of the MPSL process can be described by a model that determines the irradiation of the vat surface and its propagation into the resin, followed by a model that determines how the resin reacts to that irradiation. Schematically, the MPSL model can be given by Fig. 4.17, showing an Irradiance Model and a Cure Model.

As a given bitmap pattern is displayed, the resin imaged by the "on" mirrors is irradiated. The exposure received by the resin is simply the product of the irradiance and the time of exposure. The dimensional accuracy of an imaged part cross section is a function of the radiation uniformity across the DMD, the collimation of the beam, and the capability of the optics system in delivering an undistorted image.

If the MPSL machine's optical system produces a plane wave that is neither converging nor diverging, then it is easy to project rays from the DMD to the resin surface. The irradiance model in this case is very straightforward. However, in most practical cases, it is necessary to model the cone of rays that project from each

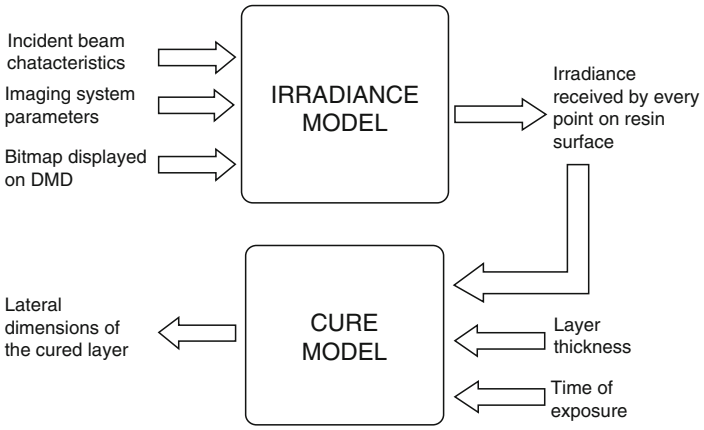

Fig. 4.17 Model of the MPSL process

micromirror on the DMD to the resin. As a result, a point on the resin may receive radiation from several micromirrors. Standard ray-tracing methods can be used to compute the irradiance field that results from a bitmap [61].

After computing the irradiance distribution on the vat surface, the cured shape can be predicted. The depth of cure can be computed in a manner similar to that used in Sect. 4.5. Cure depth is computed as the product of the resin's D_p value and the exponential of the exposure received divided by the resin's E_c value, as in (4.15). The exposure received is simply the product of the irradiance at a point and the time of exposure, T.

$$C_d = D_p e^{-E/E_c} = D_p e^{-H \cdot T/E_c} \tag{4.30}$$

In the build direction, overcure and print through errors are evident, as in SL. In principle, however, it is easier to correct for these errors than in point-wise SL systems. A method called the "Compensation Zone" approach was developed to compensate for this unwanted curing [61]. A tailored volume (Compensation Zone) is subtracted from underneath the CAD model to compensate for the increase in the Z dimension that would occur due to print-through. Using this method, more accurate parts and better surface finish can be achieved.

4.9 Two-Photon SL

In the two-photon SL (2p-SL) process, the photoinitiator requires two photons to strike it before it decomposes to form a free radical that can initiate polymerization. The effect of this two-photon requirement is to greatly increase the resolution of photopolymerization processes. This is true since only near the center of the laser is

the irradiance high enough to provide the photon density necessary to ensure that two photons will strike the same photoinitiator molecule. Feature sizes of 0.2 μm have been achieved using 2p-SL.

2p-SL was first invented in the 1970s for the purposes of fabricated three dimensional parts [62]. Interestingly, this predates the development of SL by over 10 years. In this approach, two lasers were used to irradiate points in a vat of photopolymer. When the focused laser spots intersected, the photon density was high enough for photo-polymerization.

More recently, 2p-SL received research attention in the late 1990s. A schematic of a typical research setup for this process is shown in Fig. 4.18 [63]. In this system, they used a high power Ti:Sapphire laser, with wavelength 790 nm, pulse-width 200 fs, and peak power 50 kW. The objective lens had an NA = 0.85. Similarly to other micro-SL approaches, the vat was scanned by a 3D scanning stage, not the laser beam. Parts were built from the bottom-up. The viscosity of the resin was enough to prevent the micropart being cured from floating away. Complicated parts have been produced quickly by various research groups. For example, the micro-bull in Fig. 4.19 was produced in 13 min [64]. The shell of the micro-bull was cured by 2p-SL, while the interior was cured by flood exposure to UV light.

Typical photopolymer materials can be used in 2p-SL machines [64–66]. The most commonly used resin was SCR500 from Japan Synthetic Rubber Company, which was a common SL resin in Japan, where this research started during the 1990s. SCR500 is a mixture of urethane acrylate oligomers/monomers and common free radical generating photoinitiators. The absorption spectrum of the resin shows that it is transparent beyond 550 nm, which is a significant advantage since photons can penetrate the resin to a great depth (D_p is very large). One implication is that parts can be built inside the resin vat, not just at the vat surface, which eliminates the need for recoating.

Photosensitivity of a 2p-SL resin is measured in terms of the two-photon absorption cross section (Δ) of the initiator molecule corresponding to the wavelength used to irradiate it. The larger the value of Δ, the more sensitive is the resin to two-photon polymerization, possibly enabling lower power lasers.

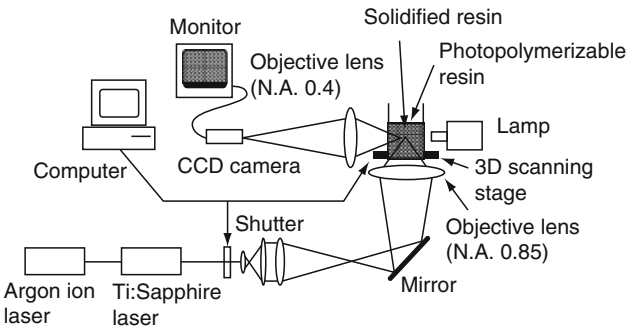

Fig. 4.18 Schematic of typical two-photon equipment

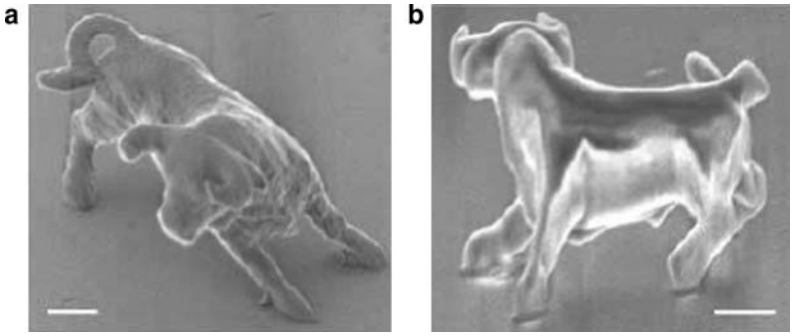

Fig. 4.19 Bull model fabricated by 2p-SL. The size scale bar is 1 μm

Acrylate photopolymer systems exhibit low photosensitivity as the initiators have small two-photon absorption cross sections. Consequently, these initiators require high laser-power and longer exposure times. Other materials have been investigated for 2p-SL, specifically using initiators with larger Δ. New types of photoinitiators tend to be long molecules with certain patterns that make them particularly good candidates for decomposing into free radicals if two photons strike it a short time apart [67]. By tuning the design of the photoinitiators, large absorption cross sections and low polymerization threshold energies can be achieved [68].

4.10 Summary

Photopolymerization processes make use of liquid, radiation-curable resins called photopolymers to fabricate parts. Upon irradiation, these materials undergo a chemical reaction to become solid. Several methods of illuminating photopolymers for part fabrication were presented, including vector scan point-wise processing, mask projection layer-wise processing, and two-photon approaches. The vector scan approach is used with UV lasers in the SL process, while DLP micromirror array chips are commonly used for mask projection technologies. Two-photon approaches, which have the highest resolution, remain of research interest only. Advantages, disadvantages, and unique characteristics of these approaches were summarized.

Photopolymerization processes lend themselves to accurate analytical modeling due to the well defined interactions between radiation and photopolymers. An extensive model for laser scan SL was presented, while a simpler one for MPSL was summarized. Discretization errors and scan patterns were covered in this chapter to convey a better understanding of these concepts as they apply to photopolymerization processes, as well as many of the processes still to be presented in this book.

4.11 Exercises

1. Explain why SL is a good process to use to fabricate patterns for investment casting of metal parts. (0.5 page+).
2. Explain why two photoinitiators are needed in most commercial SL resins. Explain what these photoinitiators do.
3. Assume you are building with the STAR-WEAVE build style under the following conditions: layer thickness = 0.006″, Dp = 6.7 mil, Ec = 9.9 mJ/cm^2 (SL-5240), machine = SLA-250/50.

   (a) Determine the cure depths C_{d1} and C_{d2} needed.
   (b) Compute the laser scan speeds required for C_{d1} and C_{d2}.
   (c) Determine laser scan speeds required C_{d1} and C_{d2} when building along an edge of the vat.

4. Assume you are building with the ACES build style under the following conditions: layer thickness = 0.004″, D_p = 4.1 mil, E_c = 11.4 mJ/cm^2 (SL-5510), machine = SLA-Viper Si2.

   (a) Determine the cure depths C_{d1} and C_{d2} needed.
   (b) Compute the laser scan speeds required for C_{d1} and C_{d2}.
   (c) Determine laser scan speeds required C_{d1} and C_{d2} when building along an edge of the vat, taking into account the laser beam angle.

5. In the derivation of exposure (4.9) for a scan from 0 to $x = b$, several steps were skipped.

   (a) Complete the derivation of (4.9). Note that the integral of e^{-v^2} from 0 to b is $\int_0^b e^{-v^2} dv = \frac{\sqrt{\pi}}{2} \text{erf}(v)\Big|_0^b$, where erf($v$) is the error function of variable v (see Matlab or other math source for explanation of erf(v)).
   (b) Compute the exposure received from this scan at the origin, at x = 10 mm, and at b = 20 mm using the conditions in Prob. 3b, where laser power is 60 mW.
   (c) Now, let b = 0.05 mm and recompute the exposure received at the origin and point b. Compare with results of part (b). Explain the differences observed.

6. Consider a tall thin rib that consists of a stack of 10 vector scans. That is, the rib consists of 10 layers and on each layer, only 1 vector scan is drawn.

   (a) Derive an expression for the width of the rib at any point z along its height.
   (b) Develop a computer program to solve your rib width equation.
   (c) Using your program, compute the rib widths along the height of the rib and plot a graph of rib width. Use the conditions of Prob. 4 and a scan speed of 1,000 mm/s.
   (d) Repeat part (c) using a scan speed of 5,000 mm/s. Note the differences between your graphs from (c) and (d).

References

1. Jacobs PF (1992) Rapid prototyping & manufacturing, fundamentals of stereolithography. Society of Manufacturing Engineers, New York, NY
2. Tang, Y (2002) Stereolithography (SL) cure modeling. Masters Thesis, School of Chemical Engineering, Georgia Institute of Technology
3. Beaman JJ, Barlow JW, Bourell DL, Crawford RH, Marcus HL, McAlea KP (1997) Solid freeform fabrication: a new direction in manufacturing. Kluwer Academic Publishers, Boston, MA
4. Hull CW (1990) Method for production of three-dimensional objects by stereolithography, 3D Systems, Inc. US Patent 4,929,402, 29 May 1990
5. Murphy EJ, Ansel RE, Krajewski JJ (1989) Investment casting utilizing patterns produced by stereolithography, DeSoto, Inc. US Patent 4,844,144, 4 July, 1989
6. Wohlers T (1991) Rapid prototyping: an update on RP applications, technology improvements, and developments in the industry. Wohlers Associates
7. Lu L, Fuh JYH, Nee AYC, Kang ET, Miyazawa T, Cheah CM (1995) Origin of Shrinkage, Distortion and Fracture of Photopolymerized Material, Materials Research Bulletin, Vol. 30, No. 12, pp 1561–1569
8. Asahi Denka JP (1988) Patent 2,138,471, filed Feb 1988
9. Asahi Denka JP (1988) Patent 2,590,216, filed Jul 1988
10. Crivello JV, Dietliker K (1998) Photoinitiators for free radical, cationic & anionic photopolymerisation, 2nd edn, Vol. III. In: Bradley G. (ed) Chemistry & technology of UV & EB formulation for coatings, inks & paints. John Wiley & Sons, Inc., Chichester & New York, in association with SITA Technology Ltd., London, UK
11. Dufour P (1993) State-of-the-art and trends in radiation curing. In: Fouassier JP, Rabek JF (eds) Radiation curing in polymer science and technology – Vol I: fundamentals and methods. Elsevier Applied Science, London & New York, p P1
12. Jacobs PF (1996) Stereolithography and other RP&M technologies. Society of Manufacturing Engineers, Dearborn, MI
13. Wilson JE (1974) Radiation chemistry of monomers, polymers, and plastics. Marcel Dekker, New York
14. Fouassier JP (1993) An introduction to the basic principles in UV curing. In: Fouassier JP, Rabek JF (eds) Radiation curing in polymer science and technology – Vol I: fundamentals and methods. Elsevier Applied Science, London & New York, p P49
15. Decker C, Elazouk B (1995) Laser curing of photopolymers. In: Allen NS et al (eds) Current trends in polymer photochemistry. Ellis Horwood, New York, p P130
16. Andrzejewska E (2001) Photopolymerization kinetics of multifunctional monomers. Prog Polym Sci 26:605
17. Hageman HJ (1989) Photoinitiators and photoinitiation mechanisms of free-radical polymerization processes. In: Allen NS (ed) Photopolymerization and photoimaging science and technology. Elsevier Science, London, p P1
18. Crivello JV (1993) Latest developments in the chemistry of onium salts. In: Fouassier JP, Rabek JF (eds) Radiation curing in polymer science and technology – Vol II: photoinitiated systems. Elsevier Applied Science, London & New York, p P435
19. Bassi GL (1993) Formulation of UV-curable coatings – how to design specific properties. In: Fouassier JP, Rabek JF (eds) Radiation curing in polymer science and technology – Vol II: photoinitiated systems. Elsevier Applied Science, London & New York, p P239
20. Crivello JV (1984) Cationic polymerization — iodonium and sulfonium salt photoinitiators. Adv Polym Sci 62:1
21. Crivello JV, Lee JL (1988) Method for making polymeric photoactive aryl iodonium salts, products obtained therefrom, and use. General Electric Company, US Patent 4,780,511, 25 Oct 1988

22. Crivello JV, Lee JL (1989) Alkoxy-substituted diaryliodonium salt cationic photoinitiators. J Polym Sci Part A: Polym Chem 27:3951–3968
23. Crivello JV, Lee JL (1990) Synthesis, characterization, and photoinitiated cationic polymerization of silicon-containing epoxy resins. J Polym Sci Part A: Polym Chem 28:479–503
24. Melisaris AP, Renyi W, Pang TH (2000) Liquid, radiation-curable composition, especially for producing flexible cured articles by stereolithography. Vantico Inc., US Patent 6,136,497, 24 Oct 2000
25. Pang TH, Melisaris AP, Renyi W, Fong JW (2000) Liquid radiation-curable composition especially for producing cured articles by stereolithography having high heat deflection temperatures. Ciba Specialty Chemicals Corp., US Patent 6,100,007, 8 Aug 2000
26. Steinmann B, Wolf JP, Schulthess A, Hunziker M (1995) Photosensitive compositions. Ciba-Geigy Corporation, US Patent 5,476,748, 19 Dec 1995
27. Steinmann B, Schulthess A (1999) Liquid, radiation-curable composition, especially for stereolithography. Ciba Specialty Chemicals Corp., US Patent 5,972,563, 26 Oct 1999
28. Crivello JV, Lee JL, Conlon DA (1983) Photoinitiated cationic polymerization with multifunctional vinyl ether monomers. J Radiat Curing 10(1):6–13
29. Decker C, Decker D (1994) Kinetic and mechanistic study of the UV-curing of vinyl ether based systems. Proc Rad Tech Conf, Orlando, vol I, p 602
30. Sperling LH (1981) Interpenetrating polymer networks and related materials. Plenum Press, New York
31. Decker C, Viet TNT, Decker D, Weber-Koehl E (2001) UV-radiation curing of acrylate/epoxide systems. Polymer 42:5531–5541
32. Sperling LH, Mishra V (1996) Polymer materials encyclopedia, vol 5. JC Salomone (ed). CRC Press, New York, p P3292
33. Chen M, Chen Q, Xiao S, Hong X (2001) Mechanism and application of hybrid UV curing system. Photogr Sci Photochem 19(3):208–216
34. Decker C (1996) Photoinitiated crosslinking polymerization. Prog Polym Sci 21:593–650
35. Decker C, Xuan HL, Viet TNT (1996) Photocrosslinking of functionalized rubber. III. Polymerization of multifunctional monomers in epoxidized liquid natural rubber. J Polym Sci Part A: Polym Chem 34:1771–1781
36. Perkins WC (1981) New developments in photo-induced cationic polymerization. J Radiat Curing 8(1):16
37. Renap K, Kruth JP (1995) Recoating issues in stereolithography. Rapid Prototyping Journal 1(3):4–16
38. Lynn-Charney CM, Rosen DW (2000) Accuracy models and their use in stereolithography process planning. Rapid Prototyping J 6(2):77–86
39. West AP (1999) A decision support system for fabrication process planning in stereolithography. Masters Thesis, Georgia Institute of Technology
40. 3D Systems web page: http://www.3dsystems.com
41. 3D Systems, Inc. (1996) AccuMax^{TM} Toolkit User Guide, 3D Systems, Inc., Valencia, CA
42. Yi F, Wu J, Xian D (1993) LIGA technique for microstructure fabrication. Microfabrication Technol 4:1
43. Ikuta K, Hirowatari K (1993) Real three dimensional microfabrication using stereolithography and metal molding. Proc. IEEE MEMS, Fort Lauderdale, FL, pp 42–47, Feb 7–10
44. Suzumori K, Koga A, Haneda R (1994) Microfabrication of integrated FMA's using stereo lithography. Proc. MEMS, Oiso, Japan, pp 136–141, Jan 25–28
45. Ikuta K, Hirowatari K, Ogata T (1994) Three dimensional micro integrated fluid systems fabricated by micro stereolithography. Proc. IEEE MEMS, Oiso, Japan, pp 1–6, Jan 25–28
46. Takagi T, Nakajima N (1994) Architecture combination by microphotoforming process. Proc. IEEE MEMS, pp 211–216
47. Ikuta K, Maruo S, Fujisawa T, Yamada A (1999) Micro concentrator with opto-sense micro reactor for biochemical IC chip family. Proc. MEMS, Orlando, FL pp 376–380, Jan 17–21

48. Gardner J, Varadan V, Awadelkarim O (2001) Microsensors MEMS and smart devices. Wiley, New York
49. Ikuta K, Ogata T, Tsubio M, Kojima S (1996) Development of mass productive microstereolithography. Proc. MEMS, San Diego, pp 301–305, Feb 11–15
50. Ikuta K, Maruo S, Fujisawa T, Fukaya Y (1998) Chemical IC chip for dynamical control of protein synthesis. Proc Int Symp Micromechatronics and Human Science, Nagoya, Japan, pp 249–254, Nov 25–28
51. Dudley D, Duncan W, Slaughter J (2003) Emerging Digital Micromirror Device (DMD) applications. Proc. SPIE, Vol. 4985, San Jose, CA, pp 14–25, Jan 28–29
52. Bertsch A, Zissi S, Jezequel J, Corbel S, Andre J (1997) Microstereolithography using liquid crystal display as dynamic mask-generator. Microsyst Technol 3(2):42–47
53. Monneret S, Loubere V, Corbel S (1999) Microstereolithography using dynamic mask generator and a non-coherent visible light source. Proc SPIE 3680:553–561
54. Chatwin C, Farsari M, Huang S, Heywood M, Birch P, Young R, Richardson J (1998) UV microstereolithography system that uses spatial light modulator technology. Appl Opt 37:7514–7522
55. Bertsch A, Bernhard P, Vogt C, Renaud P (2000) Rapid prototyping of small size objects. Rapid Prototyping Journal 6(4):259–266
56. Hadipoespito G, Yang Y, Choi H, Ning G, Li X (2003) Digital Micromirror device based microstereolithography for micro structures of transparent photopolymer and nanocomposites. Proceedings of the 14th Solid Freeform Fabrication Symposium, Austin TX, pp 13–24
57. Limaye A, Rosen DW (2004) Quantifying dimensional accuracy of a mask projection micro stereolithography system. Proc. Solid Freeform Fabrication Symposium, Austin, TX, Aug 2–4
58. Sun C, Fang N, Wu D, Zhang X (2005) Projection micro-stereolithography using digital micro-mirror dynamic mask. Sens Actuators A 121:113–120
59. Varadan VK, Jiang S, Varadan VV (2001) Microstereolithography and other fabrication techniques for 3D MEMS. Wiley, Chichester
60. V-Flash Modeler, www.modelin3d.com
61. Limaye A, Rosen DW (2006) Compensation zone approach to avoid Z errors in Mask Projection Stereolithography builds. Rapid Prototyping J 12(5):283–291
62. Swanson WK, Kremer SD (1975) Three dimensional systems. US Patent 4078229, filed 27 Jan 1975
63. Maruo S, Nakamura O, Kawata S (1997) Three-dimensional microfabrication with two-photon-absorbed photopolymerization. Opt Lett 22(2):132–134
64. Kawata S, Sun H, Tanaka T, Takada K (2001) Finer features for functional microdevices. Nature 412:697–698
65. Miwa M, Juodkazis S, Kawakami T, Matsuo S, Misawa H (2001) Femtosecond two-photon stereolithography. Applied Physics A 73:561–566
66. Sun H, Kawakami T, Xu Y, Ye J, Matsuo S, Misawa H, Miwa M, Kaneko R (2000) Real three-dimensional microstructures fabricated by photopolymerization of resins through two-photon absorption. Opt Lett 25(15):1110–1112
67. Albota M (1998) Design of organic molecules with large two-photon absorption cross sections. Science 281:1653–1656
68. Cumpston B, Ananthavel S, Barlow S, Dyer D, Ehrlich J, Erskine L, Heikal A, Kuebler S, Lee I, Mc-Cord Maughon D, Qin J, Rockel H, Rumi M, Wu X, Marder S, Perry J (1999) Two photon polymerization for three dimensional optical data storage and microfabrication. Nature 398:51–54